Supplementary information

https://doi.org/10.1631/jzus.B2500830

(a) The Auto-correlation of Selected VIs and TFs for AGB

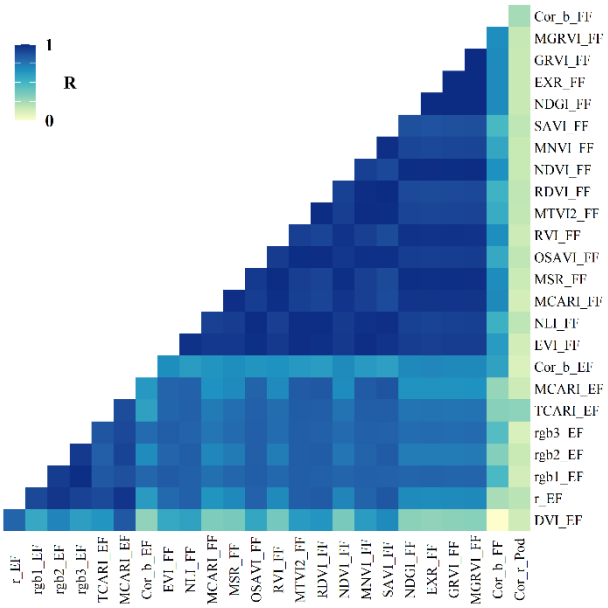

(b) The Auto-correlation of Selected VIs, TFs and SFs for Yield

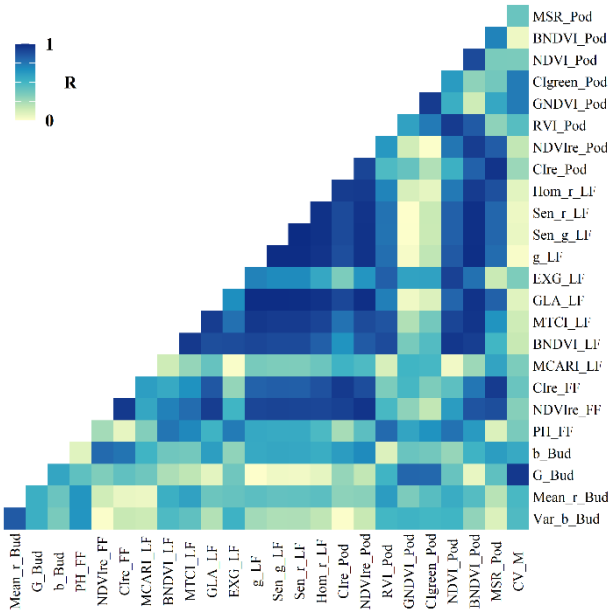

Fig. S1 Autocorrelation analysis of biomass characteristic combinations VIs-TFs and biomass characteristic combinations VIs-TFs-SFs.

Materials and methods

1.1 Experimental design

Rapeseed was transplanted on December 21, 2023 and harvested on June 2, 2024. Thirty-six plots (7 m×7 m) were established, with inter-plant spacing of 15 cm, 25 cm, and 35 cm, respectively. The four rapeseed varieties were Yangyou (YY) 9, Zhongyou (ZY) 19, Ningza (NZ) 158, and Suyou (SY) 1908. In 2024, manual sowing took place on October 17. The Detian (DT) 158 variety was manually harvested on May 18, 2025, and the remaining varieties on May 24, 2025; 108 sample plots were established (2.5 m×10 m). The rapeseed varieties were Qinyou (QY) 1718, DT 158, SY 1908, and NZ 158, with planting densities of 1.25 g/row, 1.875 g/row, and 2.5 g/row. The planting scheme for 2025 will remain consistent with that of 2024, except for the omission of the DT 158 variety. Before planting, all plots at the experimental site were applied with 375 kg/ha of green polymeric compound fertilizer. Irrigation was solely dependent on rainfall.

1.2 Data collection

For each annual experiment, above-ground biomass (AGB) and yield sampling were conducted at rapeseed maturity across all plots. In 2023, rapeseed yield was collected from the entire planting area, with a total of 36 samples collected. AGB and yield samples were collected in 2024 (36 plots×5 samples). In 2025, sampling was repeated accordingly (27 plots×3 samples). During data collection, the rapeseed plants at the plot edges were damaged. Consequently, sampling was conducted in the central three rows, with each plot further divided into five smaller subplots to ensure sample uniformity and representativeness while minimizing bias from edge effects. The fresh AGB for each plot sample was immediately measured and recorded on-site. After air-drying in the field, the rapeseed was manually threshed, and the yield was measured using an electronic scale. Table S1 presents the analysis of variance for the interaction effects of variety and density on measured biomass and yield. It is worth noting that, under drought stress in 2025, variety was not significantly correlated with rapeseed yield, whereas the correlation between planting density and yield approached significance.

Table S1 Effects of rapeseed variety, density, and their interaction on rapeseed yield and biomass

Year	Factor	Yield	Biomass
2023	Variety	0.00073	
	Density	0.86	
	Variety&Density	0.85	
2024	Variety	3.05e-10	<2e-16
	Density	0.39	0.15
	Variety&Density	0.89	0.97
2025	Variety	0.17	2.58e-10
	Density	*0.09*	0.23
	Variety&Density	0.96	0.55

Bold p-values indicate $P<0.05$, italicized p-values indicate $P<0.1$.

Unmanned aerial vehicles (UAVs) imagery was acquired, with sampling occurring approximately once a week on clear days. Phenological phases were systematically recorded and documented by researchers during each UAVs flight. Notable canopy variations were observed across distinct stages. Specifically, during the budding phase, rapid growth of the stalk and leaves was noted. After the budding stage, the yellow flowers gradually cover the entire rapeseed canopy. At the podding stage, its yield increases rapidly, while biomass remains relatively stable. Valid images were collected in 2023 (8 sets), 2024 (13 sets), and 2025 (16 sets), covering stages from budding to maturing (Table S2).

Table S2 Unmanned aerial vehicles (UAVs) and ground-based data collection

Growth Stages	Trails Dates (2023)	Trails Dates (2024)	Trails Dates (2025)	Data
Budding	March 19	February 17, March 8	February 24, March 1, March7, March11	MS Images, RGB Images
Early Flowering	March 26	March 16	March 18	
Full Flowering	April 7, April 12	March 22, March 29	March 24, March 30	
Late Flowering	April 16	April 9, April 15	April 6, April14	
Poddling	April 21	April 22, May 1	April 20, April28	
Maturing	May 8, May 14	May 8, May 15	May 7	
Harvesting	June 2	May 18, May 24	May 24	Fresh biomass, yield

MS: multispectral images.

Using sensors mounted on DJI drones, we conducted multi-year and multi-temporal image acquisition of the rapeseed canopy, capturing its spectral characteristics and structural details. UAVs images were captured around midday under clear, sunny, and windless conditions. Real-time kinematic positioning enables drones to achieve centimeter-level positioning accuracy. The flight path, heading, lateral overlap rate (85%), forward speed, and flight altitude (30 m) are consistent across all aerial surveys. A Zenmuse L1x camera, mounted on a Matrice 300 (M300) drone, was used to capture RGB images (0.33 cm/pixel). Multispectral images were acquired using a Phantom 4 multispectral (P4M) drone. The images have a half-maximum width of 16 nm, with center wavelengths at 450 nm (Red, R), 560 nm (Green, G), 600 nm (Blue, B), 730 nm (Near-Infrared, NIR), and 840 nm (Red-edge, RE) (1.6 cm/pixel).

1.3 Multidimensional feature extraction and selection

Pix4Dmapper was employed to process the multispectral and RGB images (Pix4D, Lausanne, Switzerland). A sequence of procedures was conducted, primarily involving photo alignment, the incorporation of control points, and the generation of dense point clouds. Radiometric calibration was conducted using reflectance images obtained from a reflectance calibration panel across five spectral bands. Geometric correction was conducted using ground control points (GCPs) to enhance spatial accuracy. The spectral vegatation indices (VIs) used in this study were divided into two types: those that include near-infrared, red-edge, and visible light bands, and those that cover only the visible light band (Table S3). Structural features (SFs) were extracted from crop surface model (CSM) based on the structure-from-motion algorithm (Malambo et al., 2018). Plant height (PH) was derived from CSM at the maximum percentiles. Canopy volume (CV) was calculated by multiplying each pixel's area by the corresponding PH. Additionally, texture feature (TFs) were extracted from the orthophotography RGB images. We calculated eight TFs using the "glcm" package in R software. Since RGB images consist of 3 color bands (R, G, B), a total of 24 TFs were extracted for each region of interest (ROI). The naming convention appends suffixes (_r, _g, _b) to each texture to denote the specific feature corresponding to each band.

Table S3 Spectral vegetation indices (VIs) for rapeseed yield and biomass estimation

Class	VIs	Formula	References
RGB VIs	R,G,B	Raw value of each band	/
	r	R(R+G+B)	/
	g	G(R+G+B)	/
	b	B(R+G+B)	/
	r/b	r/b	/
	r-b	r–b	/
	(r-b)/(r+b)	(r–b)/(r+b)	/
	GLA	(2G–B–R)/(2G+B+R)	(Ye et al., 2024)
	NDGI	(G–R)/(G+R)	(Zhao et al., 2020)
	MGRVI	$(g^2–r^2)/(g^2+r^2)$	(Ye et al., 2024)
	EXR	1.4×r–g	(Ye et al., 2024)
	EXG	2×g–r–b	(Ye et al., 2024)
Yield RE-NIR VIs	BNDVI	(NIR–B)/(NIR+B)	(Sulik and Long, 2016)
46	GNDVI	(NIR–G)/(NIR+G)	(Sulik and Long, 2016)
25	NDVIre	(NIR–RE)/(NIR+RE)	(Meng et al., 2025)
24	CIre	NIR/RE–1	
	CIgreen	NIR/G–1	(Meng et al., 2025)
	MTCI	(NIR–RE)/(RE–R)	(Meng et al., 2025)
	MSR	$(NIR/R–1)/(NIR/R+1)^{1/2}$	(Lu et al., 2022)
	NDVI	(NIR–R)/(NIR+R)	(Sulik and Long, 2016)
	RVI	NIR/R	(Lu et al., 2022)
	MCARI	[(RE–R)–0.2(RE–G)](RE/G)	(Meng et al., 2025)
Biomass RE-NIR VIs	TVI	60(NIR–G)–100R–G	(Meng et al., 2025)
	NLI	$(NIR^2–R)/(NIR^2+R)$	(Lu et al., 2022)
	EVI	2.5(NIR–R)/(NIR+6R–7.5B+1)	(Meng et al., 2025)
	RDVI	$(NIR–R)/(NIR+R)^{1/2}$	(Li et al., 2020)
	SAVI	1.5(NIR–R)/(NIR+R+0.5)	(Meng et al., 2025)
	OSAVI	1.16(NIR–R)/(NIR+R+0.16)	(Meng et al., 2025)
	TCARI	3[RE–R–0.2(RE–G)(RE/R)]	(Zarco-Tejada et al., 2002)
	MNVI	$1.5(NIR^2–R)/(NIR^2+R+0.5)$	(Gong et al., 2003)
	MTVI2	$1.5[1.2(NIR–G)–2.5(R–G)]/[(2NIR+1)^2–(6×NIR–5R^{1/2}–0.5)]^{1/2}$	(Meng et al., 2025)

R: Red; G: Green; B: Blue; NIR: Near-Infrared; RE: Red-edge. The bold Red-edge and Near-Infrared (RE-NIR) based VIs serve as a common index for both biomass and yield estimation

References

Gong P, Pu RL, Biging GS, et al., 2003. Estimation of forest leaf area index using vegetation indices derived from Hyperion hyperspectral data. *IEEE Trans Geosci Remote Sens*, 41(6):1355-1362. https://doi.org/10.1109/TGRS.2003.812910

Li XR, Yang CH, Huang WJ, et al., 2020. Identification of cotton root rot by multifeature selection from sentinel-2 images using random forest. *Remote Sens*, 12:3504. https://doi.org/10.3390/rs12213504

Lu LR, Luo JH, Xin YH, et al., 2022. How can UAV contribute in satellite-based *Phragmites australis* aboveground biomass estimating? *Int J Appl Earth Obs Geoinf*, 114:103024. https://doi.org/10.1016/j.jag.2022.103024

Meng L, Ming B, Liu Y, et al., 2025. Maize biomass estimation by integrating spectral, structural, and textural features from unmanned aerial vehicle data. *Eur J Agron*, 168:127647. https://doi.org/10.1016/j.eja.2025.127647

Sulik JJ, Long DS, 2016. Spectral considerations for modeling yield of canola. *Remote Sens Environ*, 184:161-174. https://doi.org/10.1016/j.rse.2016.06.016

Ye YR, Jin LP, Bian CS, et al., 2024. Estimating potato aboveground biomass using unmanned aerial vehicle RGB imagery and analyzing its relationship with tuber biomass. *Field Crops Res*, 319:109657. https://doi.org/10.1016/j.fcr.2024.109657

Zarco-Tejada PJ, Haboudane D, Miller JR, et al., 2002. Leaf chlorophyll *a*+*b* and canopy LAI estimation in crops using R-T models and Hyperspectral Reflectance Imagery. Proceedings of the VII Congress of the European Society for Agronomy.

Zhao JL, Jin Y, Ye HC, et al., 2020. Remote sensing monitoring of areca yellow leaf disease based on UAV multi-spectral images. *Trans Chin Soc Agric Eng*, 36(8):54-61 (in Chinese). https://doi.org/10.11975/j.issn.1002-6819.2020.08.007